

1 A resolved mantle anomaly as the cause of the 2 Australian-Antarctic Discordance

3 M. H. Ritzwoller, N. M. Shapiro, and G. M. Leahy¹

4 Center for Imaging the Earth's Interior, Department of Physics, University of Colorado, Boulder, Colorado, USA

5 Received 27 March 2003; revised 17 September 2003; accepted 26 September 2003; published XX Month 2003.

6 [1] We present evidence for the existence of an Australian-Antarctic Mantle Anomaly
7 (AAMA), which trends northwest-southeast (NW-SE) through the Australian-Antarctic
8 Discordance (AAD) on the Southeast Indian Ridge (SEIR), is confined to the upper
9 120 km of the mantle beneath the AAD, and dips shallowly to the west so that it extends to
10 a depth of about 150 km west of the AAD. Average temperatures within the AAMA are
11 depressed about 100°C relative to surrounding lithosphere and suggest very rapid cooling
12 of newly formed lithosphere at the AAD to an effective thermal age between 20 and
13 30 Ma. A convective down welling beneath the AAD is not consistent with the
14 confinement of the AAMA in the uppermost mantle. In substantial agreement with the
15 model of *Gurnis et al.* [1998], we argue that the AAMA is the suspended remnant of a slab
16 that subducted at the Gondwanaland-Pacific convergent margin more than 100 Myr ago,
17 foundered in the deeper mantle, and then ascended into the shallow mantle within the past
18 30 Myr, cutting any ties to deeper roots. The stability of the AAMA and its poor
19 correlation with residual topography and gravity imply that it is approximately neutrally
20 buoyant. The thermally induced density anomaly can be balanced by bulk iron depletion
21 of less than 0.8%, consistent with the warmer conditions of formation for the Pacific
22 than Indian lithosphere. We hypothesize that the low temperatures in the AAMA inhibit
23 crustal formation and the AAD depth anomaly is formed at the intersection of the SEIR
24 and the AAMA. The northward migration of the SEIR overriding the cold NW-SE
25 trending AAMA therefore presents a simple kinematic explanation for both the V-shaped
26 residual depth anomaly in the southeast Indian Ocean and the western migration of the
27 AAD along the SEIR. Neither explanation requires the Pacific asthenospheric mantle to
28 push westward and displace Indian asthenosphere. The AAMA may also act as a barrier
29 to large-scale flows in the shallow asthenosphere and may therefore define a boundary
30 for mantle convection and between the Indian and Pacific isotopic provinces. The
31 westward dip of the AAMA would also favor along-axis flow from the Indian Ocean
32 asthenosphere to the AAD that may contribute to the penetration of Indian Ocean
33 mid-ocean ridge basalts into the AAD. **INDEX TERMS:** 3035 Marine Geology and Geophysics:
34 Midocean ridge processes; 7218 Seismology: Lithosphere and upper mantle; 7255 Seismology: Surface waves
35 and free oscillations; 8180 Tectonophysics: Tomography; 9340 Information Related to Geographic Region:
36 Indian Ocean; **KEYWORDS:** Australian-Antarctic Discordance, Indian Ocean, mantle topography

37 **Citation:** Ritzwoller, M. H., N. M. Shapiro, and G. M. Leahy, A resolved mantle anomaly as the cause of the Australian-Antarctic
38 Discordance, *J. Geophys. Res.*, 108(0), XXXX, doi:10.1029/2003JB002522, 2003.

40 1. Introduction

41 [2] The Australian-Antarctic Discordance (AAD) [e.g.,
42 *Weissel and Hayes*, 1971, 1974] is a portion of the South-
43 east Indian Ridge (SEIR) between 120°E and 128°E longi-
44 tude characterized by a chaotic ridge pattern and a negative
45 depth anomaly (Figure 1). The AAD is the deepest segment
46 of the world's mid-ocean ridge system and marks a geo-

chemical boundary between Pacific and Indian type mid- 47
oceanic ridge basalts [e.g., *Klein et al.*, 1988]. Analysis of 48
local bathymetry as well as magnetic and gravity anomalies 49
shows that the AAD depth anomaly has existed for at least 50
25 Myr and during the last 20 Myr has migrated westward 51
at a rate of approximately 15 mm/yr [e.g., *Marks et al.*, 52
1999]. The geochemical boundary has also migrated west- 53
ward but apparently at a somewhat faster rate [e.g., *Pyle et al.* 54
et al., 1995]. The origin of the depth anomaly at the AAD is 55
generally attributed to colder than normal mantle temper- 56
atures below this segment of the SEIR, consistent with the 57
major element systematics for basalts from the AAD [*Klein* 58
and Langmuir, 1987]. This thermal anomaly may inhibit 59

¹Now at Geology and Geophysics Department, Yale University, New Haven, Connecticut, USA.

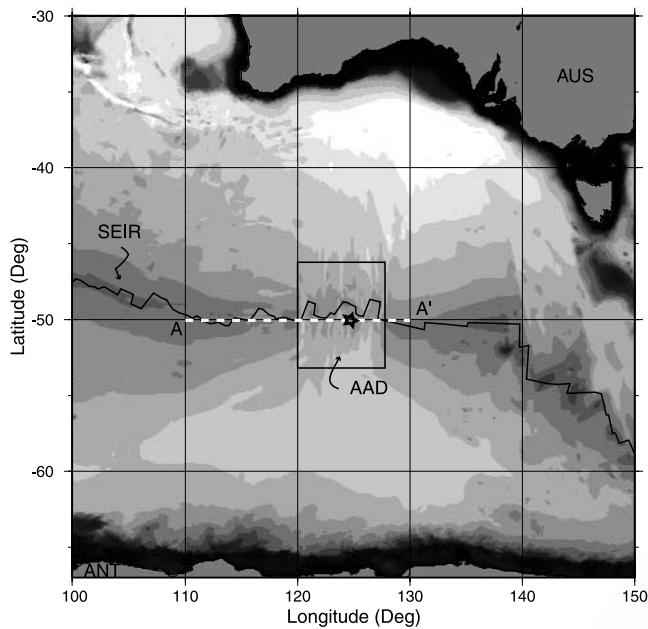


Figure 1. Bathymetric reference map of the Southeast Indian Ocean [Smith and Sandwell, 1997]. The Australian-Antarctic Discordance (AAD) region is boxed. The Southeast Indian Ridge (SEIR) cuts across the center. The star (50°S, 124°E) marks the location of the 1-D model shown in Figures 3 and 4.

60 magma production along the ridge and thin the oceanic
 61 crust [Tolstoy et al., 1995]. Several hypotheses concerning
 62 the cause of a cold mantle anomaly below the AAD have
 63 been proposed, including the existence of a stable cold spot
 64 [Hayes, 1976], convective down welling [e.g., Hayes, 1988;
 65 Klein et al., 1988], reduced upwelling [Kuo, 1993; Kuo et
 66 al., 1996], passive along-axis flow in response to colder
 67 temperatures along the ridge segment [e.g., Forsyth et al.,
 68 1987; West et al., 1997], and the presence of a stagnated
 69 slab that subducted beneath the Gondwanaland-Pacific
 70 Ridge margin and was subsequently drawn by the southeast Indian
 71 Ridge beneath the AAD [Gurnis et al., 1998]. Gurnis et al.
 72 have recently elaborated their model by presenting evidence
 73 that the AAD results specifically from the effect of an old
 74 mantle wedge [Gurnis and Müller, 2003].

75 [3] The AAD has been the subject of several previous
 76 seismic studies. Both surface wave dispersion [e.g., Forsyth
 77 et al., 1987; Kuo et al., 1996] and SS-S travel time residuals
 78 [Kuo, 1993] have shown that the upper mantle beneath the
 79 AAD is characterized by faster than normal seismic veloci-
 80 ties, which indicates that the lithosphere beneath the AAD
 81 thickens anomalously quickly and the asthenosphere is
 82 cooler than average. Global models, too, display fast upper-
 83 most mantle beneath the southeast Indian Ocean at large
 84 scales [e.g., Zhang and Tanimoto, 1993; Masters et al.,
 85 2000]. Gurnis and Müller [2003] present a detailed compar-
 86 ison between three recent global mantle models in this region.

87 [4] The purpose of the present study is to produce more
 88 detailed three-dimensional (3-D) seismic images of the
 89 upper mantle beneath the southeast Indian Ocean and
 90 surroundings to illuminate the nature and cause of the
 91 AAD. We base these images on the recent work of Ritzwoller

et al. [2001] but have expanded the data set of surface wave
 group speed dispersion measurements and have improved
 methods of surface wave inversion [Ritzwoller et al., 2002;
 Shapiro and Ritzwoller, 2002, also Thermodynamic con-
 straints on seismic inversions, submitted to *Geophysical
 Journal International*, 2003, hereinafter referred to as Sha-
 piro and Ritzwoller, submitted manuscript, 2003]. The result
 is a higher resolution and more reliable shear velocity model
 of the upper mantle beneath the southeast Indian Ocean.

[5] We present evidence for an Australian-Antarctic man-
 tle anomaly (AAMA) that is confined to the top 120 km of
 the uppermost mantle beneath the AAD and extends in the
 northwest-southeast (NW-SE) direction through the AAD.
 We argue that by affecting crustal formation, the AAMA is
 the principal cause of the AAD topographic anomaly along
 the SEIR and also plays an important role in other observ-
 ables such as the westward migration of the AAD along the
 SEIR, the V-shaped residual depth anomaly in the southeast
 Indian Ocean, and the location of a geochemical province
 boundary. Its presence and orientation provide new and
 simple kinematical explanations for a number of the char-
 acteristics that define the AAD and its surroundings.

2. Data and Surface Wave Tomography

[6] The 3-D seismic model is based on broadband surface
 wave group and phase velocity measurements. The group
 velocities were measured using the method described by
 Ritzwoller and Levshin [1998], a frequency-time method
 that involves analyst interaction to choose the frequency
 band of measurement and to guide the extraction of the
 fundamental mode from noise, scattered and multipathed
 signals, overtones, and fundamental modes of different
 wave types. We use group velocity measurements from 16
 to 200 s period for Rayleigh waves and from 16 to 150 s
 period for Love waves. We only use group velocity mea-
 surements from earthquakes shallower than 50 km to reduce
 the size of the source group time shifts, which we do not
 attempt to correct [Levshin et al., 1999]. The phase velocity
 measurements were performed at Harvard University and
 Utrecht University separately and we merged these data
 sets. The phase velocity measurements extend from 40 to
 150 s for both Rayleigh and Love waves. These data sets are
 described by Ekström et al. [1997] and Trampert and
 Woodhouse [1995]. All measurements are subjected to the
 quality control procedures described by Ritzwoller and
 Levshin [1998]. We devoted particular efforts to analyzing
 earthquakes located on the SEIR observed at SKIPPY
 stations in Australia. The resulting average path density
 for the region surrounding the AAD is shown in Figure 2a.

[7] Although we produce dispersion maps on a $2^\circ \times 2^\circ$
 grid globally [e.g., Shapiro and Ritzwoller, 2002], maps of
 the region of study are produced on a $1^\circ \times 1^\circ$ subgrid. The
 construction of the group and phase velocity maps is based
 on diffraction tomography [Ritzwoller et al., 2002], which is
 an update of the tomographic method of Barmin et al.
 [2001]. Diffraction tomography uses a simplified version of
 the scattering sensitivity kernels that emerge from the Born
 or Rytov approximations, and accounts for path length
 dependent sensitivity, wave front healing and associated
 diffraction effects, and provides a more accurate assessment
 of spatially variable resolution than traditional tomographic

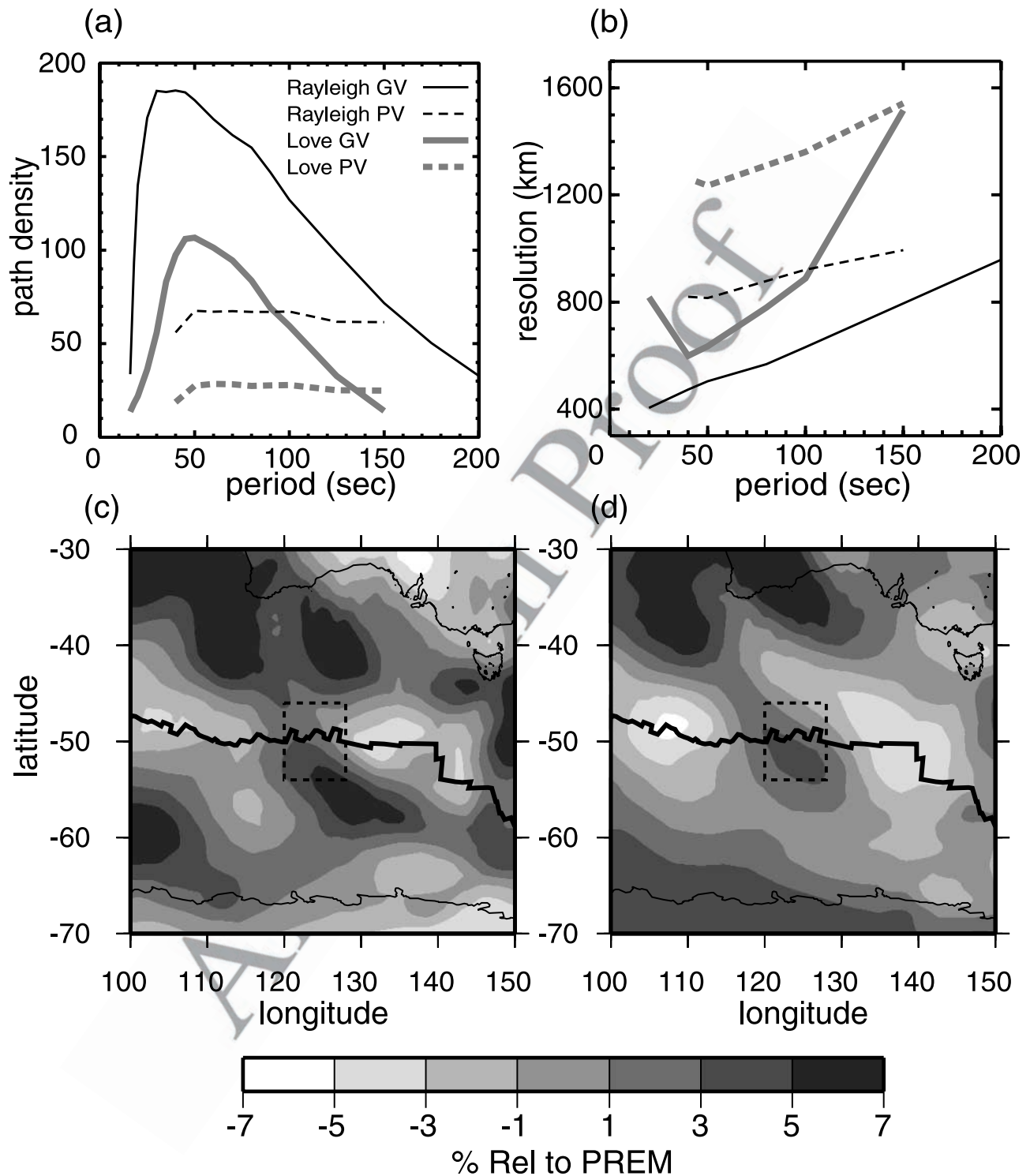


Figure 2. (a) Path density averaged over the region of study, presented as the number of paths crossing each $2^\circ \times 2^\circ$ cell (GV, group velocity; PV, phase velocity). (b) Estimated resolution averaged over the region of study. Line definition is as in Figure 2a. (c)–(d) Rayleigh wave group velocity maps shown as perturbations relative to PREM [Dziewonski and Anderson, 1981] at 45 s (Figure 2c) and 70 s (Figure 2d) periods.

152 methods based on ray theory. The resolution method is
 153 described by *Barmin et al.* [2001]. We produce a resolution
 154 surface at every node on the globe, fit a 2-D Gaussian
 155 surface in the neighborhood of each node, and define
 156 resolution as twice the standard deviation of the surface

Gaussian. Lateral resolution estimates averaged over the 157
 region of study are presented in Figure 2b. Resolution 158
 degrades with period but below 100 s, where waves are 159
 most sensitive to the uppermost mantle, Rayleigh wave 160
 resolution ranges from 400 to 700 km for group velocities 161

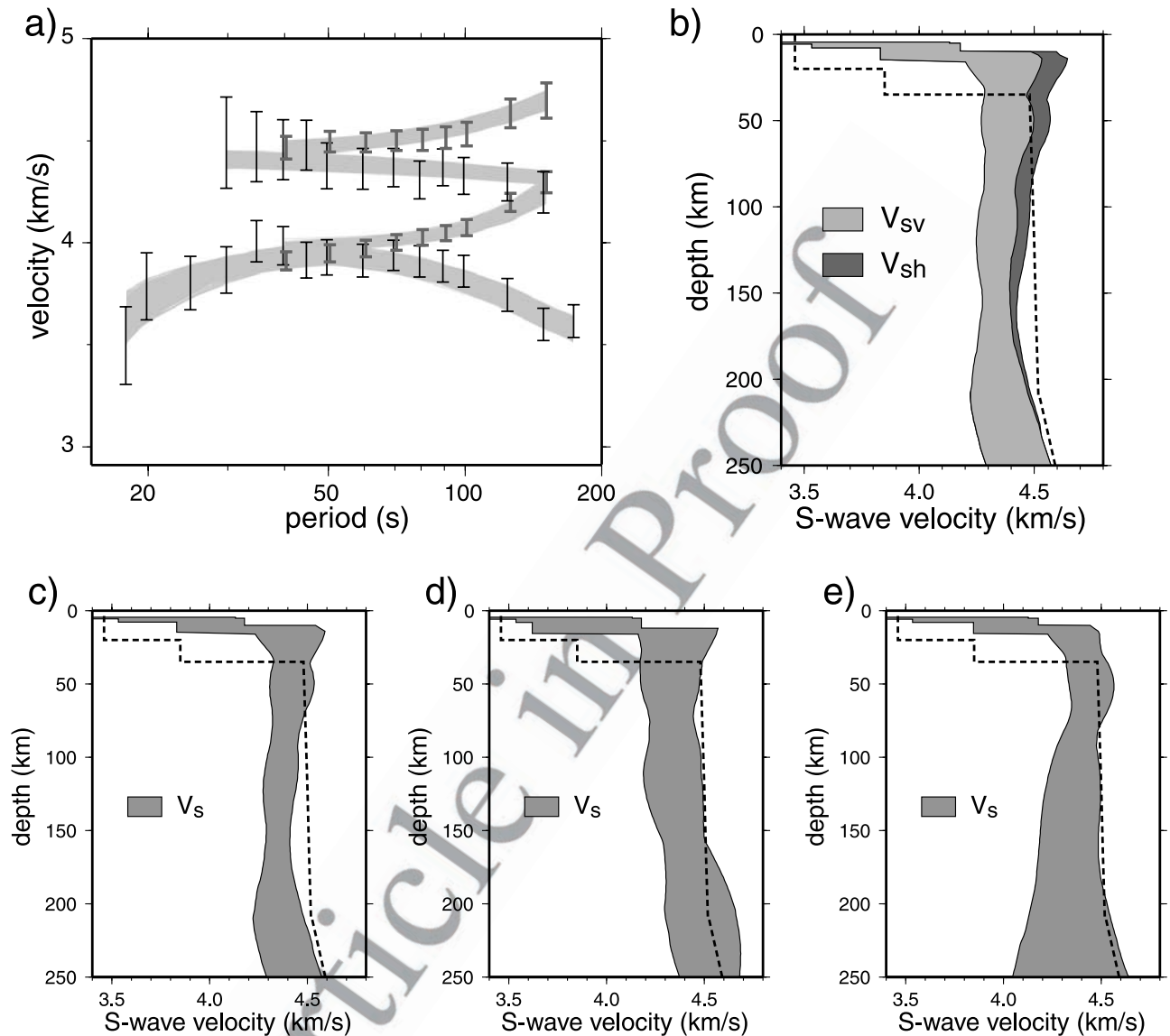


Figure 3. (a) Dispersion measurements presented as 2σ error bars obtained at the starred point in Figure 1. Dispersion curves resulting from the ensemble of acceptable models (Figure 3b) are plotted as grey lines. (b) Ensemble of acceptable models that emerge from the Monte Carlo inversion of the group and phase speed curves. The dashed line is V_s from the 1-D model ak135 [Kennett *et al.*, 1995]. (c) Ensemble of isotropic models derived from inverting group and phase speeds simultaneously, taken from the ensemble in Figure 3b where $V_s = (V_{sh} + V_{sv})/2$. (d) Same as Figure 3c, but only the phase speeds are used. (e) Same as Figure 3c, but only the group speeds are used.

162 and 800 to 900 km for phase velocities. These results will
 163 be used in a resolution test in section 4.1.

164 [8] Figures 2c and 2d show the Rayleigh wave group
 165 velocity maps at periods of 45 and 70 s, respectively. Both
 166 maps display a high-velocity anomaly that extends in the
 167 NW-SE direction through the AAD. These maps are char-
 168 acteristic of the 30–100 s range for the Rayleigh wave
 169 maps; all of which display a high-velocity anomaly trending
 170 NW-SE through the AAD.

171 **3. The 3-D Shear Velocity Model**

172 [9] The shear velocity model is constructed using a
 173 Monte Carlo method, which is described in detail by

Shapiro and Ritzwoller [2002]. The inversion is performed
 174 at each node on a $1^\circ \times 1^\circ$ grid across the region of study,
 175 and produces an ensemble of acceptable models down to a
 176 depth of 400 km. The model is constrained by a variety of
 177 priori information, including the initial crustal model
 178 CRUST2.0 (G. Laske, personal communication, 2002).
 179 *Shapiro and Ritzwoller* [2002] fully describe the set of
 180 constraints. The isotropic part of the model in the mantle
 181 is parameterized with *B* splines.
 182

[10] Figure 3 displays an example of the inversion at the
 183 starred point in Figure 1 near the center of the AAD. 184
 Measurements taken from the dispersion maps are shown
 185 in Figure 3a. The error bars are twice the RMS misfit
 186 between the dispersion measurements and the predictions
 187

188 from the dispersion maps averaged over the southern
 189 hemisphere, as described by *Ritzwoller et al.* [2001].
 190 Because of the absence of reliable uncertainty information
 191 about the dispersion maps at each point, *Shapiro and*
 192 *Ritzwoller* [2002] use this RMS misfit to weight the
 193 dispersion measurements during inversion. The RMS mis-
 194 fit between the dispersion measurements and the predic-
 195 tions from the dispersion maps, therefore, is used as a
 196 standard deviation, σ , and the error bars shown in Figure 3
 197 can be thought of as 2σ uncertainties. We find that the
 198 uncertainties, defined in this way, fairly accurately reflect
 199 at least our relative confidence in the values obtained from
 200 the dispersion maps.

201 [11] Figure 3b presents the ensemble of models that fits
 202 the observations at this point acceptably. The range of
 203 dispersion curves predicted from this ensemble is plotted
 204 over the observations in Figure 3a. The model is radially
 205 anisotropic ($V_{sh} \neq V_{sv}$) from the Moho to a variable depth
 206 that averages about 200 km. We will not discuss the
 207 anisotropic properties of the model further but will con-
 208 centrate only on the isotropic component of shear velocity
 209 ($V_s = (V_{sh} + V_{sv})/2$) at all depths. We note, however, that in
 210 the neighborhood of the AAD the general features found
 211 in V_s , V_{sh} , and V_{sv} are very similar, only the absolute
 212 values differ. The ensemble of acceptable models widens
 213 appreciably below about 200–250 km, on average, and the

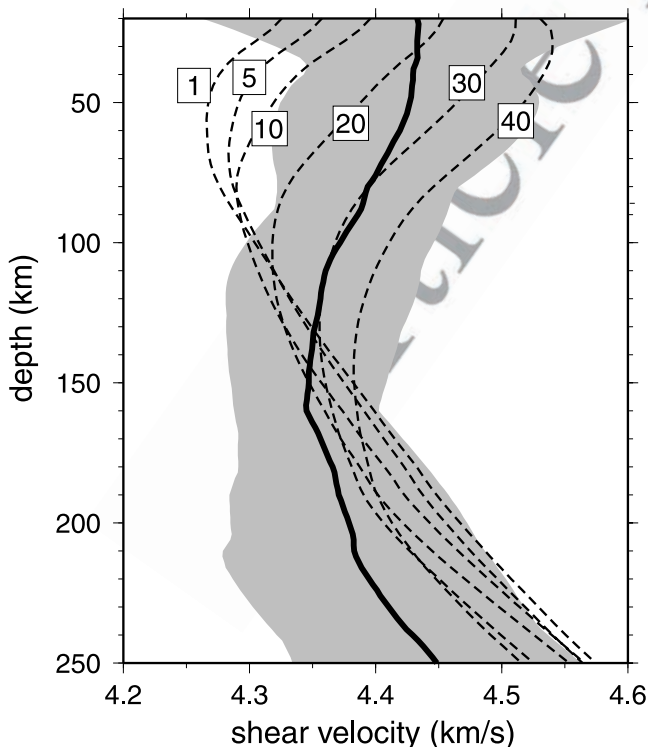


Figure 4. Age-dependent shear velocity models averaged over lithospheric age provinces in the southeast Indian Ocean plotted as dashed lines with lithospheric ages indicated in Ma. The corridor defining the ensemble of acceptable isotropic models at the AAD (the starred point in Figure 1) is presented in grey, similar to Figure 3c. The ensemble median model at this point is shown as the bold solid line.

Table 1. The χ Misfit (Equation (1)) to the Dispersion Curves at the AAD (Figure 3)

Model	All Data	Rayleigh Only	Rayleigh Group Only	
1 Ma ^a	1.80	1.82	2.21	t1.3
5 Ma ^a	1.50	1.51	1.81	t1.4
10 Ma ^a	1.29	1.29	1.53	t1.5
20 Ma ^a	1.15	1.24	1.15	t1.6
30 Ma ^a	1.95	2.20	1.77	t1.7
40 Ma ^a	2.76	3.07	2.45	t1.8
Ensemble spread ^b	0.97–1.40	1.06–1.75	0.89–1.64	t1.9
Median model ^c	1.13	1.26	1.02	t1.10

^aAge-dependent models.

^bRange from the full ensemble of acceptable models at the AAD.

^cEnsemble median model at the AAD.

model is, therefore, most reliable in the top ~ 200 km. Figures 3c–3e demonstrate the importance of simultaneously inverting the group and phase speeds. In particular, the vertical resolution of the model is substantially improved in the uppermost mantle by introducing the group speeds, which extend to shorter periods than the phase speeds. Introduction of phase speeds improves resolution below ~ 150 km. We summarize the acceptable models with a single model taken at the middle of the corridor of acceptable models. We refer to this as the ensemble median model or simply as the V_s model (e.g., the bold line in Figure 4).

[12] Because of the cooling of the oceanic crust and lithosphere after formation, the predominant feature in seismic models of the oceanic upper mantle is the formation of a lithospheric lid and the diminishment of the strength of the low-velocity zone as the lithosphere ages (e.g., Shapiro and Ritzwoller, submitted manuscript, 2003). This age-dependent trend is clear in our model of the Southeast Indian Ocean, as the lithospheric age averages in Figure 4 illustrate. These age-dependent (or age-averaged) models are computed by segregating the southeast Indian Ocean into age provinces [Müller et al., 1997] and averaging the models at each depth over each province. Anomalous topographic features such as continental shelves, the Kerguelen Plateau, the Diamantina Fracture Zone, and the AAD region were removed during the averaging of the seismic model.

[13] Misfit statistics for various models to the dispersion measurements at the AAD (Figure 4) are presented in Table 1. Misfit is normalized by the uncertainties, σ , shown in Figure 3a, defined as follows:

$$\chi - \text{misfit} = \left[\frac{1}{N} \sum_{i=1}^N \left(\frac{d_i - \hat{d}_i}{\sigma_i} \right)^2 \right]^{1/2}, \quad (1)$$

where N is the number of dispersion measurements, d is the observed group or phase speed, and \hat{d} is the group or phase speed predicted from the specified model. Of the age-dependent models, the 20 Ma model fits the dispersion data near the AAD, nearly indistinguishably from the ensemble median model.

[14] Figure 5 shows several horizontal and vertical slices of the V_s model beneath the southeast Indian Ocean. We remove the age-dependent trend (examples in Figure 4)

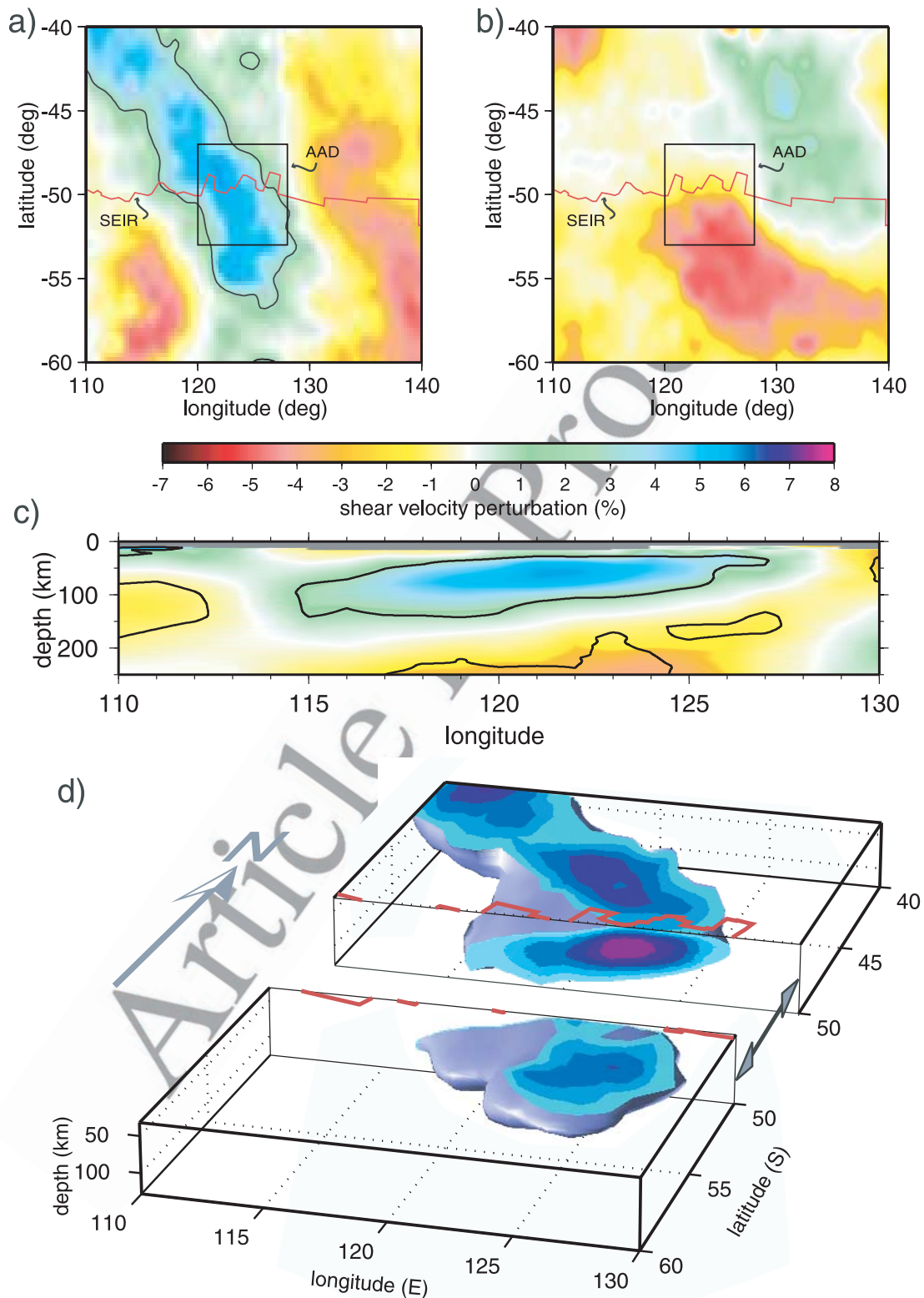


Figure 5. Images of the AAMA. (a) Horizontal slice of the V_s model at 60 km depth plotted with respect to the age-dependent model, selected age profiles of which are shown in Figure 4. Black contours indicate +3% perturbations. (b) Similar to Figure 5a, but at 200 km depth. (c) Vertical slice of the V_s model along path A-A' (Figure 1) relative to the 1 Myr age average. Black contour shows the persistent features of the model. (d) Isosurface (+2%) representation of the AAMA relative to the age-dependent model. The model was spatially smoothed somewhat to highlight the dominant large-scale features, which trend in the NW-SE direction and extend no deeper than about 120 km.

256 from these images to emphasize the features that are
 257 independent of age. The uppermost mantle beneath the
 258 AAD displays a high-velocity anomaly, relative to the age-
 259 dependent trend, to a depth of about 120 km. This Aus-
 260 tralian-Antarctic Mantle Anomaly (AAMA) extends in the
 261 northwest-southeast (NW-SE) direction through the AAD
 262 and has a gentle westward dip of about 15° relative to the
 263 horizontal along the SEIR. The Monte Carlo inversion
 264 allows us to identify the features that appear in every
 265 member of the ensemble of acceptable models. We call
 266 these features “persistent,” and as Figure 5c shows, the
 267 AAMA is only deemed persistent to a depth of about
 268 120 km beneath the AAD and somewhat deeper
 269 (~ 150 km) to the west of the AAD along the SEIR. At
 270 greater depths, this high-velocity anomaly is absent and a
 271 low-velocity anomaly eventually emerges south of the
 272 AAD as shown in Figure 5b.

273 [15] The general features of the AAMA (orientation,
 274 horizontal and depth extent, amplitude of the velocity
 275 anomaly) are quite robust relative to ad hoc choices in
 276 damping and to details of the tomographic and inversion
 277 procedures. We have, for example, also constructed models
 278 in which the surface wave tomography is based on ray
 279 theory with ad hoc Gaussian smoothing rather than diffrac-
 280 tion tomography. In addition, we constructed models in
 281 which the seismic parameterization was replaced with an
 282 intrinsically thermal parameterization (defined in section
 283 4.3). In each case we found changes in detail, but the
 284 general features of the estimated AAMA model remain
 285 substantially unchanged.

286 [16] Aspects of the AAMA have been observed previ-
 287 ously from regional surface wave studies of the southeast
 288 Indian Ocean. Using Rayleigh wave phase speeds observed
 289 at Australian stations from several events along the SEIR,
 290 Forsyth *et al.* [1987] showed that beneath young seafloor
 291 the primary anomalous feature is a lithospheric lid extend-
 292 ing at least to 40 km depth. They also showed that the low-
 293 velocity zone was less pronounced than in the Pacific,
 294 beneath crust both less than and greater than 10 Myr. These
 295 observations are in substantial agreement with the model
 296 shown in Figure 5. In a similar study based on group
 297 speeds, Kuo *et al.* [1996] argued for an elongated velocity
 298 anomaly in the uppermost mantle centered about 400 km
 299 west of the AAD and stretching northward about 1000 km.
 300 The extent of this anomaly is similar to the AAMA, but the
 301 orientation is different. The use of a larger set of regional
 302 data, in particular, measurements obtained at SKIPPY
 303 stations in Australia, has allowed us to resolve the orienta-
 304 tion of this feature, trending NW-SE through the AAD. The
 305 location of the anomaly observed on the dispersion maps is
 306 actually period dependent, and it can be misleading to infer
 307 the orientation of the mantle feature from narrow band
 308 dispersion maps alone. In particular, because the AAMA
 309 dips to the west beneath the SEIR, the high speed AAD
 310 anomaly in the dispersion maps shifts to the west as period
 311 increases. This is probably why the global model of Zhang
 312 and Tanimoto [1993], cited by Kuo *et al.* [1996], displays
 313 the high speed mantle anomaly to the west of the AAD: this
 314 global model is based only on very long period dispersion
 315 data. The AAMA shown in Figure 5 is able to fit both the
 316 short period group speed data that orient the anomaly
 317 through the AAD and the longer period dispersion measure-

ments that require the AAMA to dip to the west beneath the 318
 SEIR. 319

4. Nature and Extent of the AAMA 320

[17] cBefore considering the cause of the AAMA, we 321
 will address several preliminary issues concerning its 322
 nature and extent. The first issue relates to vertical 323
 resolution. Although the AAMA is observed to be a 324
 “persistent” anomaly only to a depth of about 120 km 325
 below the AAD, we consider the possibility that the 326
 anomaly extends to significantly greater depths but the 327
 surface waves simply do not resolve it. The second issue 328
 concerns how the seismic (and presumably thermal) struc- 329
 ture beneath the AAD compares to normal oceanic litho- 330
 sphere across the southeast Indian Ocean, particularly as a 331
 function of lithospheric age. This issue relates to how the 332
 lithosphere forms and evolves beneath and adjacent to the 333
 AAD. Finally, the third issue concerns whether the AAMA 334
 is entirely a temperature anomaly. We consider evidence 335
 that the AAMA is also compositionally distinct from the 336
 surrounding mantle. 337

4.1. Depth Extent of the AAMA 338

[18] The range of models that emerge from the Monte 339
 Carlo inversion reflects uncertainties associated with the 340
 limited and variable depth sensitivity of the surface waves. 341
 It does not, however, account for the diminishment of lateral 342
 resolution with depth caused by the reduction of resolution 343
 at long periods, as seen in Figure 2b. Therefore the deeper 344
 features of the model at the length scales of the AAMA 345
 (< 1000 km) are significantly less robust than the shallower 346
 features. It remains to be determined if the AAMA could, in 347
 fact, extend to depths greater than ~ 120 km. 348

[19] To address this issue, we created a 2-D synthetic 349
 model with a fast slab-like anomaly of Gaussian cross 350
 section in the upper mantle. The characteristics of this 351
 synthetic anomaly (amplitude, width, and dip angle) reflect 352
 the observed properties of the AAMA, except the feature 353
 extends down to the transition zone (Figure 6a). The slab 354
 anomaly plotted in Figure 6a is added to the 1 Myr average 355
 model for the southeast Indian Ocean (Figure 4). The 356
 dispersion curves for this synthetic model are inverted using 357
 the same Monte Carlo method applied to the real data. The 358
 results of the inversion, presented Figure 6b, show that 359
 the slab-like feature is well recovered all the way to the 360
 transition zone. To account for the effects of the variation of 361
 lateral resolution with period and wave type, a second 362
 inversion was performed in which the synthetic dispersion 363
 curves were smoothed horizontally to mimic the estimated 364
 resolution shown in Figure 2b. The results of this second 365
 test are shown in Figure 6c. Although the recovered 366
 anomaly widens with depth due to the degradation in 367
 resolution at long periods, a fast anomaly is apparent to 368
 depths well below the 120 km depth that we argue is the 369
 greatest depth to which the AAMA extends. Note that the 370
 results presented here are for V_{sv} for which lateral resolution 371
 is better than either V_{sh} or V_s . Similar results are seen in V_{sh} 372
 or V_s but the broadening with depth is greater in these 373
 velocities. 374

[20] These resolution tests show that the continuation of 375
 the AAMA to depths greater than about 120 km is not likely 376

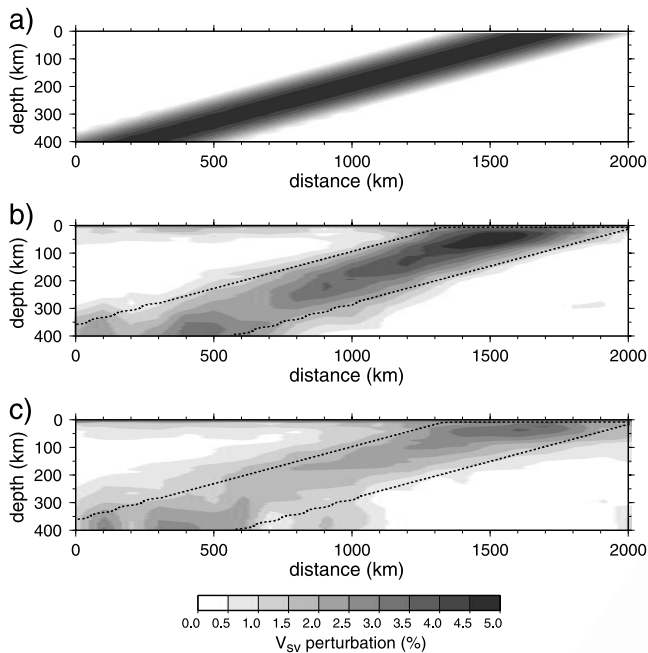


Figure 6. Synthetic resolution test. (a) Synthetic input model of a high-velocity anomaly extending into the transition zone. This perturbation is taken relative to the 1 Myr age model. (b) Model estimated with the Monte Carlo inversion of the synthetic phase and group velocities computed from the model in Figure 6a. (c) Model estimated from synthetic phase and group velocity maps that have been smoothed laterally to match the estimated period and wave type dependent resolution (Figure 2b). The dotted lines in Figures 6b and 6c outline the input structure.

377 unless the deeper reaches of the anomaly have significantly
 378 smaller amplitudes than the shallower parts. We are confi-
 379 dent, therefore, that the AAMA is largely confined to the
 380 top 120 km of the upper mantle beneath the AAD, although
 381 it dips somewhat deeper to the west. It may, however, be
 382 underlain in the transition zone and uppermost lower mantle
 383 by a high-velocity anomaly, as revealed by recent global
 384 mantle images [e.g., *Masters et al.*, 2000]. We discuss the
 385 possibility of a genetic relationship between these anomalies
 386 in section 5. As in any inversion, the AAMA may be
 387 sharper and its amplitude may be larger than our tomo-
 388 graphic images reflect.

389 **4.2. Comparison of Mantle Beneath the AAD With**
 390 **“Normal” Oceanic Mantle**

391 [21] We use two different methods to assess how mantle
 392 structure beneath the AAD compares with other nonanom-
 393 alous oceanic lithosphere across the southeast Indian Ocean.

394 **4.2.1. Similarity Analysis**

395 [22] The first method is a direct comparison between the
 396 model at the AAD with the model at other locations. We
 397 define the “similarity” S between a model at two points in
 398 space, $v(z)$ and $v_{\text{ref}}(z)$, as the depth integrated weighted one-
 399 norm difference between the two 1-D profiles:

$$S = 1 - N^{-1} \int \sigma^{-1}(z) |v(z) - v_{\text{ref}}(z)| dz, \quad (2)$$

where $N = \int dz$ and $\sigma(z)$ is the uncertainty in the reference
 401 model v_{ref} at depth z defined by the half width of the
 402 ensemble of acceptable models. The limits on the integrals
 403 are 20 and 130 km, respectively. S lies between 0 and 1 for
 404 similar vertical profiles; in particular, $S = 1$ for identical
 405 profiles. If $S < 0$, we consider the two 1-D profiles to be
 406 dissimilar. Similarity is reminiscent of two-point correlation,
 407 but two perfectly correlated models will be dissimilar if they
 408 are offset by an appreciable constant velocity.

[23] An example is shown in Figure 7 in which the
 410 reference profile is taken at the starred location within
 411 the AAD shown in Figure 1. The grey shaded regions are
 412 the parts of the southeast Indian Ocean mantle that are
 413 similar to the mantle beneath the AAD. On average, the
 414 upper mantle beneath the AAD is similar to the parts of the
 415 southeast Indian Ocean outside the AAD region with
 416 lithospheric ages ranging from about 15 to 30 Ma.
 417

418 **4.2.2. Thermal Parameterization of Mantle Structure**

[24] The second method to compare mantle structure
 419 beneath the AAD with lithosphere underlying the rest of
 420 the southeast Indian Ocean is based on the thermal model
 421 parameterization described by Shapiro and Ritzwoller (sub-
 422 mitted manuscript, 2003). In this method, the seismic
 423 parameterization used to define the model shown in Figure
 424 5 is replaced by an intrinsically thermal model (Figure 8a)
 425 in which a conductive layer is underlain by a mantle
 426

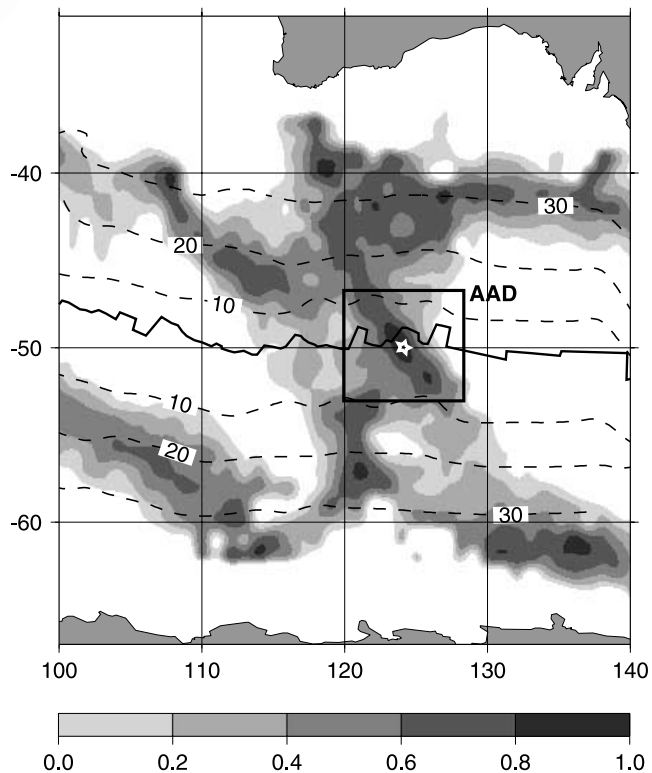


Figure 7. Similarity, defined by equation (2), between the mantle model beneath the AAD (starred point) and the rest of the southeast Indian Ocean upper mantle. Darker grey shades indicate stronger similarity to the mantle beneath the AAD. Lithospheric age isochrons are shown as dashed lines. Results are for the model with the seismic parameterization.

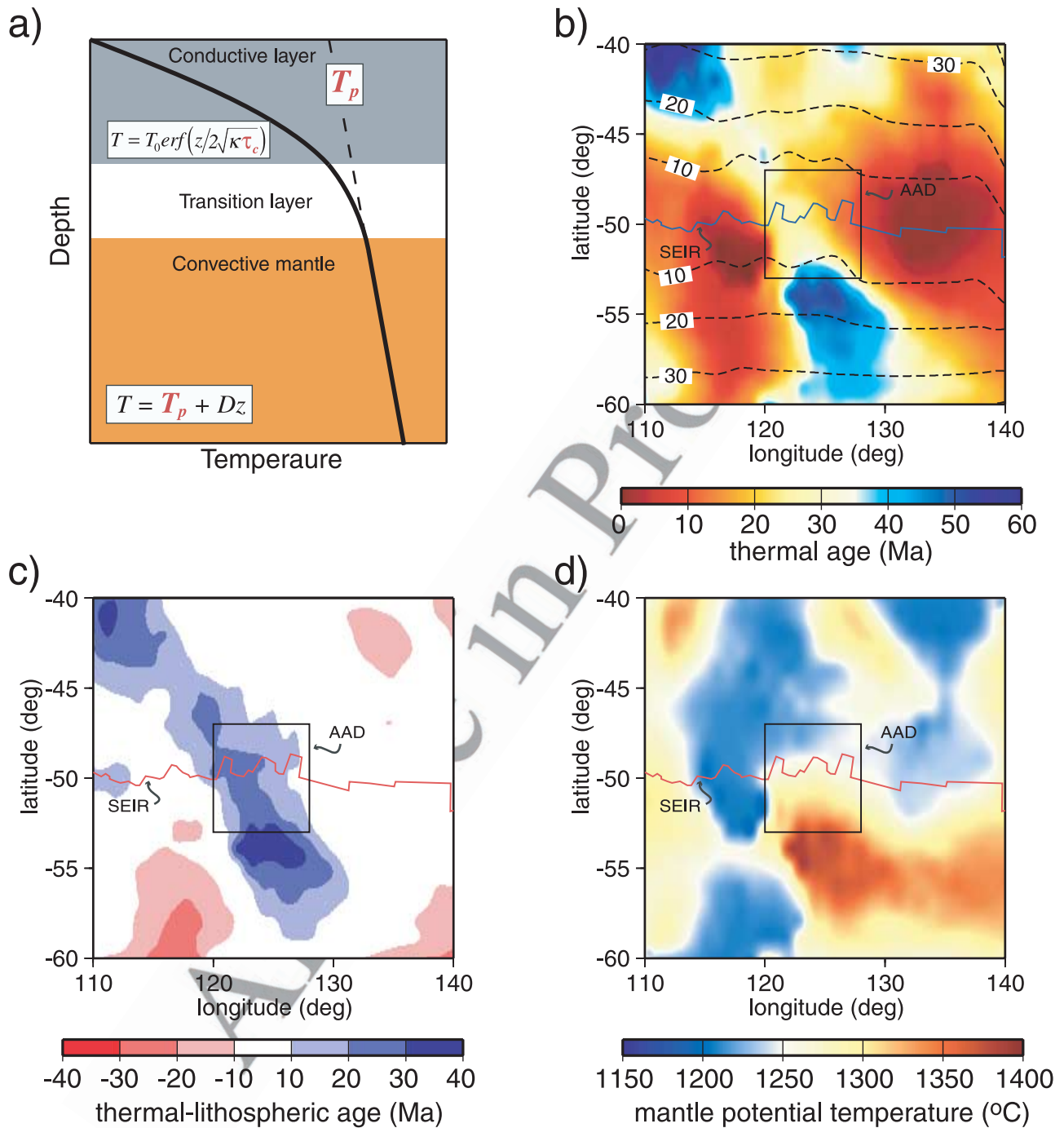


Figure 8. Results of the inversion with the thermal parameterization of the oceanic lithosphere for comparison with results using the seismic parameterization. (a) Thermal parameterization is defined by a conductive layer, described by thermal age τ_c , underlain by a convecting asthenosphere described by the mantle adiabat which is represented by potential temperature T_p . (b) Estimated apparent thermal age, τ_c , across the southeast Indian ocean lithosphere. Isochrons of lithospheric ages are plotted as dashed lines. (c) Difference between thermal age and lithospheric age. The entire AAMA, including the region of the AAD, is much cooler than its lithospheric age would suggest. (d) Estimated mantle potential temperature, T_p , of the southeast Indian ocean asthenosphere.

427 adiabat. Although this thermal model is most appropriate for
 428 nonanomalous oceanic lithosphere, we believe that results
 429 in the neighborhood of the AAD are meaningful even
 430 though the AAD is an anomalous ridge segment. The
 431 thermal parameterization is used here exclusively as a

consistency check on the results obtained from the similar- 432
 analysis applied to the model derived using the seismic 433
 parameterization. All figures here except Figure 8 originate 434
 from the seismic parameterization and all inferences can 435
 derive from the seismic parameterization alone. Neverthe- 436

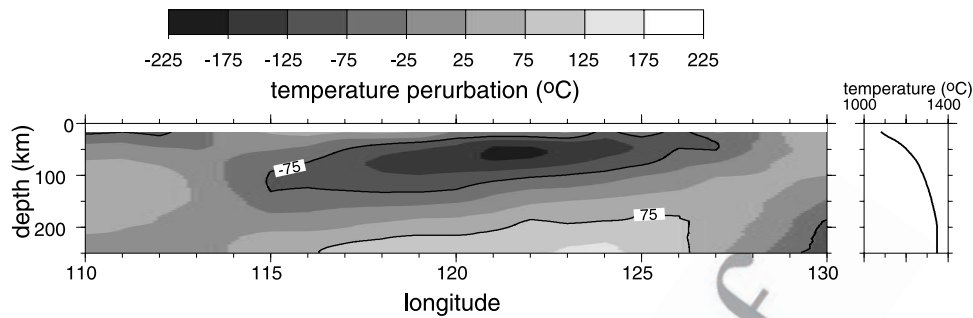


Figure 9. Temperature variations beneath profile A-A' in Figure 1, taken relative to the average temperature profile along the SEIR, shown at right. Temperatures are computed from the model with the seismic parameterization shown in Figure 5c.

less, as we show, the results with the thermal parameterization agree with those from the seismic parameterization and confirm the results of the similarity analysis.

[25] In the thermal model, temperatures within the conductive layer are given by an error function whose characteristics are determined by its apparent thermal age, τ_c , and within the convective mantle by the potential temperature, T_p . The apparent thermal age summarizes the structure of the lithosphere and potential temperature represents asthenospheric structure. The coefficient of thermal diffusivity, κ , and the adiabatic gradient, D , are assumed to be known within the mantle. Therefore the mantle temperature profile is determined by only two unknowns, τ_c and T_p . The Monte Carlo inversion proceeds as with the seismic parameterization, except that models are randomly generated in temperature space and converted to isotropic shear velocity using a mineralogical model of average oceanic composition [Dick *et al.*, 1984], laboratory-measured thermoelastic properties of individual minerals, the Voigt-Reuss-Hill averaging scheme, and an anelastic model. This conversion is based on the method of Goes *et al.* [2000] and is described in detail by Shapiro and Ritzwoller (submitted manuscript, 2003). After converting each candidate thermal model to isotropic shear velocity, radial anisotropy with randomly chosen strength and depth extent is introduced, so each candidate shear velocity model is radially anisotropic between the Moho and about 200 km depth, as with the seismic parameterization discussed above. Candidate models are promoted into the acceptable category if they satisfactorily fit the dispersion information. We report here ensemble averages for τ_c and T_p .

[26] The estimated apparent thermal age across the southeast Indian Ocean is shown in Figure 8b. The thermal age of the AAD is seen to be elevated relative to the rest of the SEIR. Figure 8c demonstrates that the thermal age at the AAD is between 20 and 30 Myr greater than expected for newly formed lithosphere. This “excess thermal age” follows the strike of the AAMA NW-SE through the AAD. Figure 8d shows the potential temperature beneath the southeast Indian Ocean. Similar to Figure 5b, this demonstrates that asthenospheric temperatures on the Antarctic Plate to the south of the AAD are elevated.

[27] The conclusion from both the similarity analysis and the thermal parameterization (i.e., thermal age estimates) is that the seismic and temperature structures of the lithosphere beneath the AAD more nearly resemble 20–30 Ma

lithosphere than the lithosphere beneath normal spreading ridges. This conclusion also agrees well with evidence provided by Forsyth *et al.* [1987] that phase speeds beneath young lithosphere where the residual depth anomaly is greater than 500 m are significantly elevated relative to Pacific seafloor of comparable age.

4.3. Is the AAMA a Purely Thermal Anomaly?

[28] Using the conversion between temperature and shear velocity discussed in section 4.2, we convert the 3-D model derived using the seismic parameterization into temperature and density. The resulting temperature anomalies along the SEIR are shown in Figure 9. The lowest temperature anomaly beneath the AAD is about 200°C at 60 km depth, but the spatial average of the temperature depression within the AAMA is about 100°C with respect to a regional average. This average is similar to the mean temperature anomaly reported in previous studies, although individual earlier estimates varied substantially between studies [e.g., Forsyth *et al.*, 1987; Klein and Langmuir, 1987; Hayes, 1988; Forsyth, 1992; Kuo, 1993; Shen and Forsyth, 1995; Sempere *et al.*, 1997; West *et al.*, 1997; Gurnis *et al.*, 2000]. The low temperatures beneath the AAD are qualitatively consistent with the AAD depth anomaly and suggest a rapid cooling of newly formed lithosphere to an effective thermal age of between 20 and 30 Ma. To be believed, the density anomalies that result from these low temperatures must be consistent with seafloor topography as well as the apparent long-term stability of the AAMA over at least the past 25 Myr.

[29] Density anomalies are computed from the temperatures shown in Figure 9 using a coefficient of thermal expansion $\alpha = 3.0 \times 10^{-5} \text{ K}^{-1}$. These anomalies can be used to compute the relative bathymetry Δh along the SEIR assuming isostatic compensation in the mantle:

$$\Delta h = \frac{1}{\rho_m - \rho_w} \int_{z_0}^{z_c} (\rho(z) - \rho_{\text{ref}}(z)) dz, \quad (3)$$

where z_c is the depth of compensation (chosen to be 130 km), z_0 is fixed at 20 km to avoid the crustal contribution, $\rho(z)$ is the density profile of the column in question, and ρ_m and ρ_w are average densities of the mantle and water, respectively. The reference mantle density, ρ_{ref} , is chosen to minimize the average difference between the predicted and observed topography along the SEIR. It is,

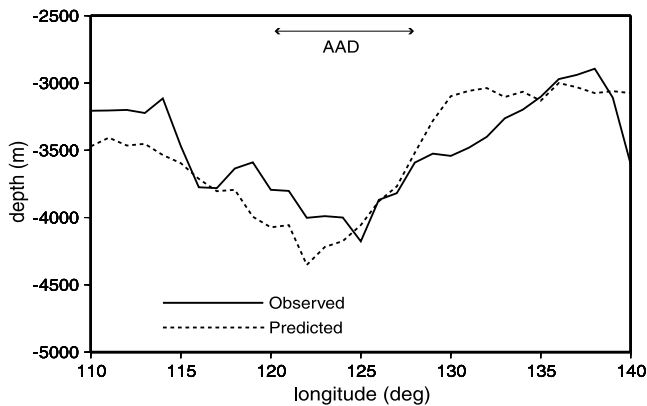


Figure 10. Comparison between the observed topography along profile A-A' in Figure 1 and that predicted assuming isostatic compensation from the temperature model shown in Figure 9. The predicted topography has been shifted vertically to match the average observed topography. Results are for the model with the seismic parameterization.

525 therefore, only the variation in topography that is predicted
526 by the seismic model. This prediction of topography derives
527 exclusively from the mantle contribution down to a depth of
528 130 km; the crust is assumed to be laterally homogeneous
529 and does not contribute to the relative topography.

530 [30] The mantle contribution to bathymetry along 50°S
531 predicted in this way from the 3-D shear velocity model fits
532 the shape and the magnitude of the observed bathymetry
533 rather well, as Figure 10 shows. It is tempting therefore to
534 hypothesize that the AAMA is a purely thermal anomaly
535 that is dense, intrinsically negatively buoyant, and isostati-
536 cally compensated by topography on the sea floor beneath
537 the SE Indian Ocean.

538 [31] There are several problems with this hypothesis,
539 however. First, if we would correct the observed bathymetry
540 for crustal thickness variations along the SEIR, the topog-
541 raphy would become strongly overpredicted. *Tolstoy et al.*
542 [1995] present evidence that the crust within the AAD is
543 about 3 km thinner than along the adjacent ridge segments.
544 This would accommodate more than half of the observed
545 topography anomaly. Therefore either the temperature
546 anomalies shown in Figure 9 are too large by about a factor
547 of two or the AAMA beneath the AAD is supported by
548 some other means. Given uncertainties in the V_s -to-temper-
549 ature conversion, the temperature anomalies in Figure 9
550 may, in fact, be overestimated, but there are three other
551 severe problems for the hypothesis. Second, the AAMA
552 does not correlate with the V-shaped off-ridge residual
553 depth anomalies beneath the southeast Indian Ocean as
554 shown in Figure 11. Only at the AAD is the AAMA
555 coincident with residual depth anomalies. It is therefore
556 unlikely that the AAMA is compensated isostatically by
557 seafloor topography in a general sense across the southeast
558 Indian Ocean. Third, there is no pronounced geoid or long-
559 wavelength gravity anomaly associated with the AAMA.
560 Given the absence of topographic anomalies northwest of
561 the AAD, if the AAMA is denser than surrounding mantle it
562 should have a clear gravity signature. Finally, if it is the
563 cause of the AAD, the AAMA must have existed in the
564 uppermost mantle at least as long as the AAD, i.e., for

>25 Myr. If the AAMA is as dense as predicted under the
assumption of the very cool temperatures shown in Figure 9
with average Indian oceanic composition, it must be sup-
ported by some other means in order to be nearly neutrally
buoyant.

[32] One way to explain these observations is that the
AAMA is not in isostatic equilibrium but is dynamically
supported. Although this alternative cannot be ruled out, we
see no direct evidence for low seismic velocities (hence,
high temperatures) underlying the full extent of the AAMA,
although high temperatures can be inferred beneath the
AAMA on the Antarctic Plate south of the SEIR. It is
possible, however, that the compensation is deeper than the
~200–250 km depth to which our 3-D model extends.
However, the greater the depths of the supporting anomaly,
the less likely it will be to produce the relatively sharp
topographic features needed to compensate for the topog-
raphy that the AAMA would impart isostatically to the
seafloor.

[33] A more plausible possibility is that the AAMA is not
purely a thermal anomaly but is compositionally distinct
from normal mantle beneath the southeast Indian Ocean.

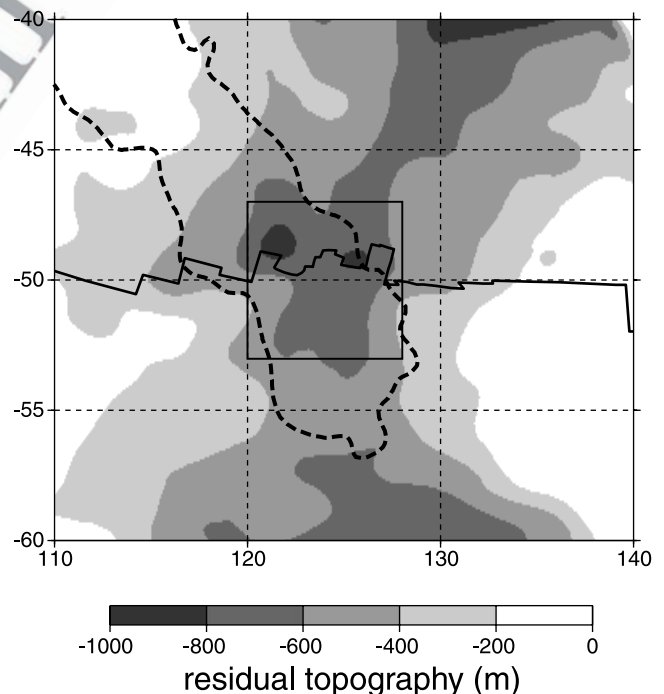


Figure 11. Residual topography (dh) compared with the 3% contour (dashed line) of the AAMA at 60 km depth (taken from Figure 5a). Residual topography is the difference between the topography estimated by *Smith and Sandwell* [1997], which we refer to as “observed”, and topography predicted from seafloor age A in Ma: $dh = 2620 \text{ m} - 350 \sqrt{A} \text{ m}$. Both the observed and predicted topography are smoothed using a spatial Gaussian filter with a standard deviation of 70 km. The observed topography is corrected isostatically for sedimentary load taken from the crustal model of G. Laske and G. Masters (personal communication, 2002). The residual depth anomaly (dark grey shades) forms a V-shaped feature that is poorly correlated with the AAMA except at the SEIR.

587 More specifically, the AAMA may be composed of mantle
 588 minerals that are more depleted in heavier elements than
 589 surrounding mantle. The density perturbations caused by
 590 the compositional and thermal anomalies approximately
 591 balance, but the effects on the seismic wave speeds are
 592 additive. As a result, the AAMA is seismically fast, but may
 593 be approximately neutrally buoyant. This will be discussed
 594 further in section 5.

596 5. Cause and Implications of the AAMA

597 [34] We have presented evidence for the existence of an
 598 Australian-Antarctic Mantle Anomaly (AAMA) that trends
 599 NW-SE through the Australian-Antarctic Discordance
 600 (AAD), is confined to the upper 120 km of the mantle
 601 beneath the AAD, and dips shallowly to the west so that it
 602 extends to a depth of about 150 km west of the AAD. We
 603 have also shown that lithospheric structure beneath the
 604 AAD resembles normal oceanic lithosphere with ages
 605 between 20 and 30 Ma. Finally, we have argued that in
 606 the absence of deeper dynamical support, the AAMA must
 607 be approximately neutrally buoyant. Thus the AAMA is
 608 not purely thermal in origin but is probably also compo-
 609 sitionally distinct from surrounding mantle such that the
 610 thermally induced density anomalies are approximately
 611 balanced by depletion in heavy elements. How, then, has
 612 the AAMA formed and what are the implications for other
 613 observables?

614 5.1. AAMA as a Suspended Slab Remnant

615 [35] It has been often proposed that the AAD is caused by
 616 convective down welling in response to along-axis astheno-
 617 spheric flow [e.g., *Veevers*, 1982; *Vogt et al.*, 1984; *Klein et al.*,
 618 1988; *Marks et al.*, 1990, 1991; *Kuo*, 1993; *Sempere et al.*,
 619 1997; *West et al.*, 1997]. The confinement of the AAMA
 620 within the top 120 km of the uppermost mantle beneath the
 621 AAD makes this hypothesis unlikely, however. This does
 622 not prohibit the presence of mass-preserving passive along-
 623 axis flows in response to the cool temperatures in the
 624 uppermost mantle beneath the AAD, but a cold convective
 625 current penetrating the mantle beneath the AAD does not
 626 appear consistent with the seismic evidence.

627 [36] We argue that the AAMA is a stagnated remnant of a
 628 subducted slab, as argued by *Gurnis et al.* [1998]. As shown
 629 in Figure 12, the observed temperature anomalies of up to
 630 200°C are consistent with temperatures likely to exist in a
 631 diffusively heated slab that subducted more than 100 Myr
 632 ago. Whether this calculation is relevant to AAMA depends
 633 on the means by which the slab remnant was transported
 634 toward the surface. This calculation may reflect the thermal
 635 state of the AAMA if the anomaly detached and rose as a
 636 single piece from depth. If, however, the anomaly was
 637 extruded upward, perhaps from a thin layer near the surface
 638 of the foundered slab in the transition zone or uppermost
 639 lower mantle, the relevance of this calculation is question-
 640 able. Whatever the nature of transport, the AAMA appears
 641 to be lying nearly horizontally in the uppermost mantle,
 642 being thinner vertically (~100 km) than in either horizontal
 643 direction (~500 km east-west, ~200 km north-south). In
 644 particular, it shows no sign of attachment to a deeper root
 645 extending into the transition zone or lower mantle. Deeper
 646 roots may have once existed and, in fact, there is evidence

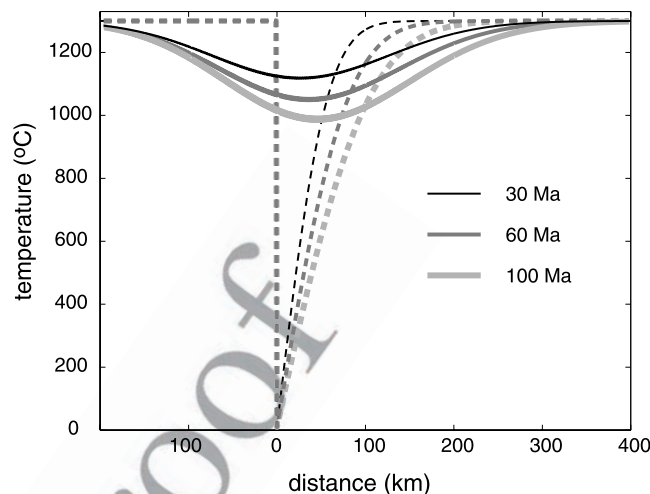


Figure 12. Initial and final temperature profiles for a 1-D slab heated diffusively along two sides. Dashed lines are the initial temperature profiles (error functions) for oceanic lithosphere that begins to subduct at the specified ages: 30, 60, and 100 Ma. Solid lines are the final temperature profiles after 150 Myr of heating. Peak internal temperature anomalies of up to 200°C are consistent with a slab subducted at the Pacific-Gondwanaland margin and heated diffusively for more than 100 Myr.

for their existence now [e.g., *Masters et al.*, 2000], but the
 AAMA is not now attached to them.

649 5.2. Westward Migration of the AAD

650 [37] If the AAMA were deeply rooted, its motion pre-
 651 sumably would be controlled by the flow regime of the
 652 transition zone or lower mantle. Because it is not attached to
 653 a deeper root, however, the AAMA is free to move with the
 654 large-scale tectonic motions that characterize the region.
 655 Superimposed on the relative motion of Australia away
 656 from Antarctica, at a rate of about 7 cm/yr, is the motion of
 657 Australia and Antarctica to the east at a speed of about 3–
 658 4 cm/yr in the hot spot reference frame [e.g., *Gurnis et al.*,
 659 1998]. It is plausible that the AAMA is now moving in lock
 660 step with these features to the east, but remains approxi-
 661 mately fixed between Australia and Antarctica as they move
 662 apart. There is a potential problem, however, for the
 663 comotion of the AAMA to the east with Australia and
 664 Antarctica. *Gurnis et al.* present a compelling argument that
 665 during the Cretaceous, Australia overrode a slab that sub-
 666 ducted at the Gondwanaland-Pacific convergent margin and
 667 foundered in the transition zone. At least during the Creta-
 668 ceous, then, this slab moved independently of Australia,
 669 was deep enough in the mantle so that the Australian
 670 cratonic keel could override it and was probably controlled
 671 by a deeper mantle flow regime that differed from the
 672 surface motions of Australia. If the AAMA is a remnant
 673 of this slab, it would have only risen to its current shallow
 674 location in the uppermost mantle after it was completely
 675 overridden by Australia. *Lin et al.* [2002] discuss how the
 676 rifting of Australia off of Antarctica may have produced
 677 substantial updrafts in the uppermost mantle. These updrafts
 678 may have contributed to the ascent of the AAMA. Indeed,
 679 using 3-D convection calculations as a function of time with

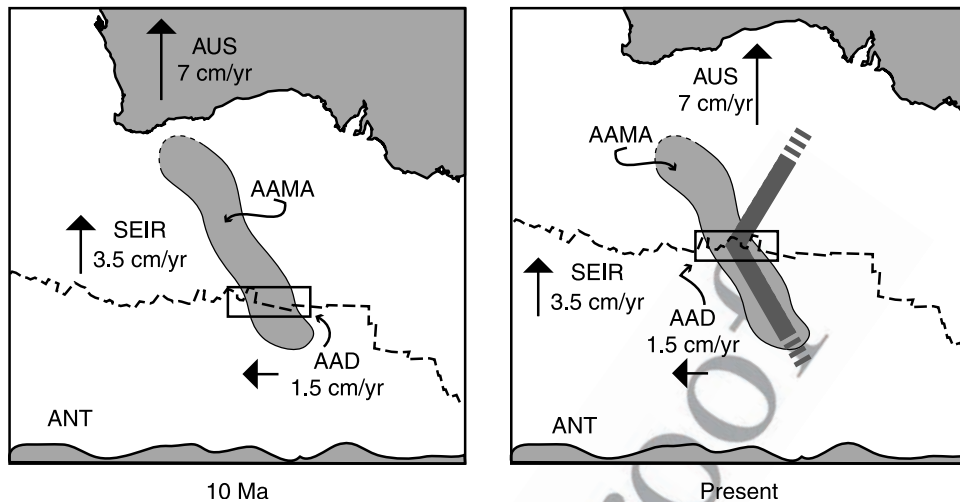


Figure 13. Plate kinematic explanation of the observed westward migration of the AAD and the V-shaped topographic anomaly in the SE Indian Ocean. Assuming that the AAD lies at the intersection of the SEIR and the AAMA, as the SEIR migrates northward at 3.5 cm/yr, the AAD will migrate westward at about 1.5 cm/yr relative to the ridge. If the topographic anomaly is frozen into the crust, it will form a V-shaped feature (shown with thick grey lines) as the AAD moves to the west relative to the SEIR.

680 observed plate motions, Gurnis et al. established that
681 updrafts are expected to entrain deep seated material, and
682 provide a mechanism of transport toward the surface. The
683 reconstruction of Gurnis et al. places the emergence of the
684 relict slab from beneath Australia at about 30 Ma. It is
685 reasonable to postulate that during its ascent, the foundered
686 slab detached from any deeper mantle roots and emerged
687 into the large-scale flow regime of Australia, Antarctica,
688 and the southeast Indian Ocean where it is currently
689 suspended.

690 [38] In this case, the orientation of the AAMA, trending
691 NW-SE through the AAD, provides a simple explanation
692 for the westward migration of the AAD based purely on
693 plate kinematics. If the AAD is caused by anomalously cool
694 mantle directly beneath the spreading center, then it should
695 originate at the intersection of the AAMA and the SEIR.
696 The SEIR is migrating northward from Antarctica at about
697 3.5 cm/yr [DeMets et al., 1994]. If the location and
698 orientation of the AAMA are approximately fixed in the
699 mantle with Antarctica, the intersection of the AAMA and
700 the SEIR would migrate westward at about 1.5 cm/yr as the
701 SEIR moves northward, as shown in Figure 13. This is in
702 rough agreement with the observed westward motion of the
703 AAD [e.g., Marks et al., 1999].

704 5.3. Thermal and Compositional State of the AAMA

705 [39] We have argued that the AAMA is the suspended
706 remnant of a slab that subducted at the Gondwanaland-
707 Pacific convergent margin more than 100 Myr ago, founde-
708 red in the transition zone, and ascended into the shallow
709 mantle within the past ~30 Myr. The AAMA should,
710 therefore, be compositionally similar to subducted Pacific
711 lithosphere, unless it underwent partial melting in the
712 transition zone or on its ascent to the uppermost mantle.
713 Studies of mid-ocean ridge basalts [e.g., Klein and Lang-
714 muir, 1987] and abyssal peridotites [e.g., Dick et al., 1984]
715 reveal significant compositional variations in the upper
716 mantle beneath mid-oceanic ridges attributed to different

melting conditions beneath the ridges. Below relatively hot
717 ridges, the degree of melting is higher and the residual
718 mantle is more highly depleted in the basaltic component
719 and in heavier elements, such as iron. Both geochemical
720 data and the seafloor depth indicate that at present, the
721 mantle is warmer beneath the East Pacific Rise than the
722 SEIR [Klein and Langmuir, 1987]. Therefore the Pacific
723 lithosphere is likely to be depleted in heavy elements
724 compared with the Indian Ocean lithosphere. We hypothe-
725 size that the Pacific lithosphere that subducted at the
726 Gondwanaland-Pacific convergent margin ~150 Myr ago
727 is more similar to the present-day Pacific lithosphere than to
728 the Indian lithosphere. Therefore interpreting the AAMA as
729 the remnant of old subducted Pacific lithosphere suggests
730 that it is compositionally distinct from the surrounding
731 Indian-type upper mantle. In particular, under this interpre-
732 tation, the AAMA is likely to be depleted in heavy elements
733 relative to the Indian Ocean lithosphere.
734

[40] The stability of the AAMA and its lack of correlation
735 with residual topography and gravity is, therefore, attributed
736 to near-neutral buoyancy that results from a balance
737 between low temperatures and depletion in heavy elements,
738 particularly iron: $\alpha\rho\Delta T \approx (\partial\rho/\partial X_{Fe})\Delta X_{Fe}$. Here $\alpha \approx 3.0 \times$
739 10^{-5}K^{-1} is the coefficient of thermal expansion [Saxena
740 and Shen, 1992], $\rho \approx 3.3 \times 10^3 \text{kg/m}^3$ is density, ΔT
741 is the temperature anomaly, ΔX_{Fe} is iron depletion, and
742 $\partial\rho/\partial X_{Fe} \approx 1200 \text{kg/m}^3$ [Duffy and Anderson, 1989]. The
743 bulk iron depletion needed to balance the, on average,
744 100°C temperature anomalies shown in Figure 9, would,
745 therefore, be about 0.8% with an uncertainty of about
746 half this value. This compositional heterogeneity would
747 have only a relatively small influence on seismic velocities:
748 $(\partial v_s/\partial X_{Fe}) \Delta X_{Fe} < 0.5\%$, if $X_{Fe} < 1\%$, taking the partial
749 derivative from Goes et al. [2000].
750

[41] Although Johnson et al. [1990] show that iron/
751 magnesium ratios may vary between individual samples
752 of abyssal peridotites by up to 3%, Dick et al. [1984]
753 present evidence for aggregated trends in iron content
754

755 between ridge segments in the Indian and Atlantic Oceans
756 to be a little more than 1%. A bulk iron depletion of 0.8%
757 within the AAMA may therefore be somewhat higher than
758 is likely to occur. If the temperature anomalies in Figure 9
759 are overestimated, however, then the requisite iron depletion
760 would be proportionally reduced.

761 [42] We conclude that the AAMA is approximately neu-
762 trally buoyant and the average temperature depression
763 within the AAMA is probably somewhat less than 100°C.
764 The thermally induced density anomaly is approximately
765 balanced by the bulk depletion in iron of <0.8%.

766 [43] Previous estimates of temperature anomalies beneath
767 the AAD segregate according to the method used, with
768 geophysically (largely seismically) determined temperature
769 depressions typically being larger (100°C–250°C) than
770 those estimated geochemically (60°C–150°C). Figure 9
771 may illuminate the cause of this difference: the largest
772 temperature anomalies do not reside in the shallowest
773 mantle. As argued by *West et al.* [1997], the geochemical
774 estimates reflect temperatures in the melting region which is
775 in the shallowest mantle. We estimate that the average
776 temperature anomaly in the upper mantle beneath the
777 AAD is probably no larger than 100°C, but the temperature
778 depression in the shallowest mantle is less than this average
779 and the maximum temperature depression, which lies at
780 about 60 km depth in our model, is substantially greater.

781 5.4. Crustal Formation and Residual Topography

782 [44] Geochemical evidence [e.g., *Klein et al.*, 1991]
783 establishes the AAD as a region with a low degree of partial
784 melting as well as lower melt production and supply and
785 agrees with seismic evidence [*Tolstoy et al.*, 1995] that the
786 crust is thin. It is likely that the depressed temperatures
787 within the AAMA inhibit melt production and provide the
788 root cause of these phenomena, at least in a large-scale
789 spatially averaged sense. The poor correlation between the
790 AAMA with residual topography off the SEIR implies that
791 topographic anomalies, both along the SEIR and off axis,
792 owe their existence to processes involved in the formation
793 of the crust. Because processes of crustal formation occur at
794 spatial scales much smaller than the resolution of our model,
795 we do not anticipate a detailed correlation between the
796 complex of topographic features that exist along the SEIR
797 (ridge segmentation, chaotic topography, propagating
798 ridges, etc.) with the AAMA. In a spatially averaged sense,
799 however, we believe that residual depth anomalies are
800 locally compensated by thinned crust and perhaps very light
801 uppermost mantle and, in particular, do not result from
802 convective down welling because the AAMA is approxi-
803 mately neutrally buoyant. *Gurnis et al.* [2000], in a com-
804 prehensive discussion about crustal formation and mantle
805 temperatures from a dynamical modeling standpoint, argue
806 that about half of the residual topography results from
807 crustal thinning. Our evidence suggests, however, that
808 topography is essentially controlled by crustal thinning, at
809 least at the spatial scales of the seismic model.

810 [45] The 800 m of anomalous topography relative to
811 adjoining ridge segments, therefore, would require crustal
812 thinning of about 4.5 km. Although this is somewhat larger
813 than reported by *Tolstoy et al.* [1995], using the arguments
814 of *Langmuir et al.* [1992], who estimate the crust will thin
815 by about 60 m for each 1°C decrease in average mantle

816 temperature beneath the ridge, the temperature anomalies
817 shown in Figure 9 are in general agreement with this value.
818 For example, at 122°E the average temperature depression
819 in the top 175 km beneath the ridge is about 80°C relative to
820 the adjacent ridge segments outside the AAD. These cool
821 temperatures would generate about 4.8 km of crustal thin-
822 ning using the methods from *Langmuir et al.* [1992].

823 [46] The uncertainties in each of the values used in this
824 calculation (amplitude of temperature anomaly, depth inter-
825 val of integration, partial derivative of crustal thickness with
826 respect to temperature anomaly) are too large to give the
827 results much credence, but we believe these calculations do
828 establish the reasonableness of the hypothesis that at large
829 spatial scales crustal thickness controls the residual depth
830 anomaly. Resolution of this issue will await more extensive
831 seismic studies performed in the neighborhood of the AAD
832 to estimate crustal thickness.

833 [47] In our view, therefore, residual topography origi-
834 nates at the intersection of the AAMA with the SEIR due
835 to inhibition of crustal formation. As discussed in section
836 5.2, the northward migration of the SEIR causes the AAD
837 to move northwest along the strike of the AAMA (i.e.,
838 west in the frame of the ridge). As a result, as new crust
839 forms the depth anomaly will move off the ridge axis,
840 producing a V-shaped “wake” in the bathymetry of the
841 southeast Indian Ocean as the AAD migrates westward
842 along the SEIR. This is illustrated in Figure 13b.

843 [48] Aspects of this argument were foreseen by *Klein et al.*
844 [1988] and *Gurnis et al.* [1998], who discussed the effect of
845 the SEIR ridge moving north over a “cold line” in the
846 mantle. The cold line for *Klein et al.* was a convective down
847 welling and for *Gurnis et al.* it was a relict slab, but both
848 imagined the feature oriented north-south through the AAD,
849 for want of better information. *Gurnis et al.* hypothesized
850 that the westward migration of the AAD and the V-shaped
851 residual depth anomaly result from the motion of Australia
852 and Antarctica to the east in the hot spot reference frame
853 while the cold line remained approximately fixed. Others
854 have argued that these features result from the westward
855 migration of Pacific Ocean asthenosphere into Indian Ocean
856 asthenosphere [e.g., *Lanyon et al.*, 1995]. These are essen-
857 tially the same argument presented from different frames of
858 reference: the hot spot frame and the frame of the SEIR,
859 respectively. We have argued above, however, that the
860 AAMA is very shallow and is detached from deeper roots,
861 so it is comoving with Australia and Antarctica to the east
862 with respect to the hot spot frame. The V-shaped residual
863 topography, therefore, does not require the invasion
864 of Pacific oceanic asthenosphere into the Indian oceanic
865 asthenosphere from the east. It results rather from the
866 formation of anomalously thin crust at the intersection of
867 the AAMA and the SEIR, the northward migration of the
868 SEIR, and the NW-SE orientation of the AAMA, which
869 could not have been foreseen by previous researchers.

870 5.5. Consequences on Mantle Flow and a Geochemical 871 Province Boundary

872 [49] The existence of a 500 km × 1500 km cold mantle
873 anomaly in the uppermost mantle that is compositionally
874 distinct from the surrounding lithosphere will affect mantle
875 flow. Although significant progress has been made in
876 simulating the dynamical conditions that formed the AAD

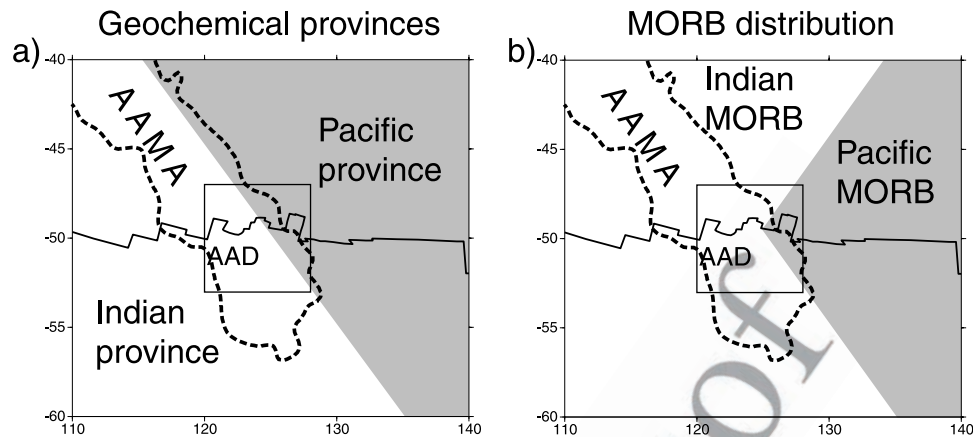


Figure 14. (a) Schematic representation of the AAMA acting as a boundary between Pacific and Indian geochemical provinces in the mantle. The dashed line marks the boundary of the AAMA at 60 km depth. (See Figure 5a). (b) Potential distribution of MORBs (Indian type, Pacific type) extruded at the surface as the SEIR moves northward and the AAD moves northwestward along the strike of the AAMA. This could be misinterpreted as Pacific asthenosphere penetrating into and displacing Indian asthenosphere along the SEIR.

877 [e.g., West et al., 1997; Gurnis et al., 1998, 2000; Gurnis
 878 and Müller, 2003; Lin et al., 2002], full understanding of
 879 large-scale convection between Australia and Antarctica
 880 will await dynamical simulations that model the origin
 881 and effects of the AAMA, including its geometry and depth
 882 extent. In lieu of these models, three observations are worth
 883 noting. First, although the compositional anomaly will
 884 probably have little dynamical effect, by increasing viscosity
 885 the cool temperatures will tend to inhibit flows through
 886 the AAMA beneath the AAD. As a consequence, the
 887 AAMA will act as a barrier to east–west flows within the
 888 upper asthenosphere and may, indeed, mark a mantle
 889 convection boundary as proposed by Klein et al. [1988],
 890 although the boundary will not be characterized by a down
 891 welling. The boundary will exist not only at the AAD, but
 892 will also extend NW–SE through the AAD along the strike
 893 of the AAMA. Second, although the AAMA will obstruct
 894 east–west flows, its westward dip may also affect the
 895 passive transport of asthenospheric material to the AAD.
 896 Figure 9 reveals that mantle temperatures are cooler toward
 897 the east end of the AAD, as isotherms generally dip to the
 898 west. Along-axis flows in the asthenosphere will be more
 899 efficiently obstructed from the Pacific Ocean side, yielding
 900 predominant along-axis asthenospheric flows from the west.
 901 This may contribute to Indian mid-ocean ridge basalts
 902 (MORBs) penetrating nearly to the eastern end of the
 903 AAD. Christie et al. [2001] have shown that the Indian–
 904 Pacific geochemical boundary follows the eastern side of
 905 the AAD depth anomaly along the SEIR. Third, as a
 906 boundary to convection, the AAMA may also mark a
 907 boundary separating Pacific and Indian type geochemical
 908 provinces. Although the AAMA may be the province
 909 boundary in the mantle, the isotopic distribution observed
 910 in basalts will approximately follow a V-shaped trend
 911 similar to the residual depth anomalies. This is consistent
 912 with the observation that the Indian–Pacific isotopic bound-
 913 ary does not continue directly northward from the AAD
 914 [e.g., Lanyon et al., 1995]. North and east of the AAD, then,
 915 Indian Ocean MORBs may, in fact, overlie Pacific type

mantle, as shown in Figure 14. In any event, in this region
 one needs to be careful in inferring mantle geochemistry
 from the overlying MORBs.

[50] The relevance of some of these comments depends on
 the extent to which the large-scale features of the AAMA
 affect magma generation and transport. If magma transport
 is largely in the shallowest mantle and is strongly affected by
 structures such as ridge segmentation that are not resolvable
 in the seismic model, then the large-scale seismic model may
 be of limited help in unraveling the details of the distribution
 of MORBs across the southeast Indian Ocean. In addition, as
 it currently appears [e.g., Pyle et al., 1995], the MORB
 boundary and the residual depth anomaly that marks the
 locus of points that were once at the AAD, may not coincide.
 This may be because mantle structures with different length
 scales and that occur at different depths affect topography
 and basalt chemistry differently. Nevertheless, more com-
 plete sampling of MORBs across the southeast Indian Ocean
 is crucial in helping to determine the effect of the AAMA on
 the convective state of the upper mantle.

[51] **Acknowledgments.** This paper benefited from critical reviews
 from David Christie, Michael Gurnis, and Ban-Yuan Kuo. We would like to
 thank the staffs of the IRIS-DMC and the GEOSCOPE data center for
 providing most of the waveform data on which the dispersion measure-
 ments were obtained. We thank Shi-Jie Zhong for many valuable con-
 versations. We are also particularly grateful to Jeannot Trampert at Utrecht
 University and Michael Antolik, Adam Dziewonski, and Goran Ekström at
 Harvard University for providing phase speed measurements and to Robert
 van der Hilst and Brian Kennett for donating waveform data from the
 SKIPPY and KIMBA arrays in Australia. The SKIPPY and KIMBA data
 sets were collected by the Research School of Earth Sciences, Australian
 National University, and greatly improved the quality of the dispersion
 maps at short and intermediate periods. All maps were generated with the
 Generic Mapping Tools (GMT) data processing and display package
 [Wessel and Smith, 1991, 1995]. This work was supported by grants from
 the Office of Polar Programs at the U.S. National Science Foundation, NSF-
 OPP-9615139 and NSF-OPP-0125848.

References

Barmin, M. P., M. H. Ritzwoller, and A. L. Levshin, A fast and reliable
 method for surface wave tomography, *Pure Appl. Geophys.*, 158, 1351–
 1375, 2001.

- Christie, D. M., et al., Mantle reservoirs and migration associated with Australian-Antarctic rifting, Leg 187 summary, *Proc. Ocean Drill. Program Initial Rep.*, 187, 1–49, 2001.
- DeMets, C., R. G. Gordon, D. F. Argus, and S. Stein, Effect of recent revisions to the geomagnetic reversal time scale on estimates of current plate motions, *Geophys. Res. Lett.*, 21, 2191–2194, 1994.
- Dick, H. J. B., R. L. Fisher, and W. B. Bryan, Mineralogic variability of the uppermost mantle along mid-oceanic ridges, *Earth Planet. Sci. Lett.*, 69, 88–106, 1984.
- Duffy, T. S., and D. L. Anderson, Seismic velocities in mantle minerals and the mineralogy of the upper mantle, *J. Geophys. Res.*, 94, 1895–1912, 1989.
- Dziewonski, A. M., and D. L. Anderson, Preliminary Reference Earth Model, *Phys. Earth Planet. Inter.*, 25, 297–356, 1981.
- Ekström, G., J. Tromp, and E. W. F. Larson, Measurements and global models of surface waves propagation, *J. Geophys. Res.*, 102, 8137–8157, 1997.
- Forsyth, D. W., Geophysical constraints on mantle flow and melt generation beneath mid-ocean ridges, in *Mantle Flow and Melt Generation at Mid-Ocean Ridges*, *Geophys. Monogr. Ser.*, vol. 71, edited by J. Phipps Morgan, D. Blackman, and J. Sinton, pp. 1–65, AGU, Washington, D. C., 1992.
- Forsyth, D. W., R. L. Ehrenbard, and S. Chapin, Anomalous upper mantle beneath the Australian-Antarctic Discordance, *Earth Planet. Sci. Lett.*, 84, 471–478, 1987.
- Goes, S., R. Govers, and P. Vacher, Shallow mantle temperatures under Europe from P and S wave tomography, *J. Geophys. Res.*, 105, 11,153–11,169, 2000.
- Gurnis, M., and R. D. Müller, The origin of the Australian-Antarctic Discordance from an ancient slab and mantle wedge, *The Evolution and Dynamics of the Australian Plate*, *Geol. Soc. Aust. Spec. Publ.*, 22, 422–423, 2003.
- Gurnis, M., R. D. Muller, and L. Moresi, Cretaceous vertical motion of Australia and the Australian-Antarctic Discordance, *Science*, 279, 1499–1504, 1998.
- Gurnis, M., L. Moresi, and R. D. Müller, Models of mantle convection incorporating plate tectonics: The Australian region since the Cretaceous, in *The History and Dynamics of Global Plate Motions*, *Geophys. Monogr. Ser.*, vol. 121, edited by M. A. Richards, R. Gordon, and R. van der Hilst, pp. 211–238, AGU, Washington, D. C., 2000.
- Hayes, D. E., Nature and implications of asymmetric sea-floor spreading - Different rates for different plates, *Geol. Soc. Am. Bull.*, 87, 994–1002, 1976.
- Hayes, D. E., Age-depth relationships and depth anomalies in the southeast Indian Ocean and South Atlantic Ocean, *J. Geophys. Res.*, 93, 2937–2954, 1988.
- Johnson, K. T., H. J. B. Dick, and N. Shimizu, Melting in the oceanic upper mantle: An ion microprobe study of diopsides in abyssal peridotites, *J. Geophys. Res.*, 95, 2661–2678, 1990.
- Kennett, B. L. N., E. R. Engdahl, and R. Buland, Constraints on seismic velocities in the Earth from travel times, *Geophys. J. Int.*, 122, 108–124, 1995.
- Klein, E. M., and C. H. Langmuir, Global correlation of ocean ridge basalt chemistry with axial depth and crustal thickness, *J. Geophys. Res.*, 92, 8089–8115, 1987.
- Klein, E. M., C. H. Langmuir, A. Zindler, H. Staudigel, and B. Hamelin, Isotope evidence of a mantle convection boundary at the Australian-Antarctic Discordance, *Nature*, 333, 623–629, 1988.
- Klein, E. M., C. H. Langmuir, and H. Staudigel, Geochemistry of basalts from the southeast Indian Ridge, 115°E–138°E, *J. Geophys. Res.*, 96, 2089–2107, 1991.
- Kuo, B.-Y., Thermal anomalies beneath the Australian-Antarctic Discordance, *Earth Planet. Sci. Lett.*, 119, 349–364, 1993.
- Kuo, B.-Y., C.-H. Chen, and Y.-S. Zhang, A fast velocity anomaly to the west of the Australian-Antarctic Discordance, *Geophys. Res. Lett.*, 23, 2239–2243, 1996.
- Langmuir, C. H., E. M. Klein, and T. Plank, Petrological systematics of mid-ocean ridge basalts: Constraints on melt generation beneath ocean ridges, in *Mantle Flow and Melt Generation at Mid-Ocean Ridges*, *Geophys. Monogr. Ser.*, vol. 71, edited by J. Phipps Morgan, D. Blackman, and J. Sinton, pp. 183–280, AGU, Washington, D. C., 1992.
- Lanyon, R., A. J. Crawford, and S. M. Eggins, Westward migration of the Pacific Ocean upper mantle into the Southern Ocean region between Australia and Antarctica, *Geology*, 23, 511–514, 1995.
- Levshin, A. L., M. H. Ritzwoller, and J. S. Resovsky, Source effects on surface wave group travel times and group velocity maps, *Phys. Earth Planet. Inter.*, 115, 293–312, 1999.
- Lin, S.-C., L.-Y. Chiao, and B.-Y. Kuo, Dynamic interaction of cold anomalies with the mid-ocean ridge flow field and its implications for the Australian-Antarctic Discordance, *Earth Planet. Sci. Lett.*, 203, 925–935, 2002.
- Marks, K. M., P. R. Vogt, and S. A. Hall, Residual depth anomalies and the origin of the Australian-Antarctic Discordance, *J. Geophys. Res.*, 95, 17,325–17,338, 1990.
- Marks, K. M., D. T. Sandwell, P. R. Vogt, and S. A. Hall, Mantle downwelling beneath the Australian-Antarctic Discordance zone: Evidence from geoid height versus topography, *Earth Planet. Sci. Lett.*, 103, 325–338, 1991.
- Marks, K. M., J. M. Stock, and K. J. Quinn, Evolution of the Australian-Antarctic Discordance since Miocene time, *J. Geophys. Res.*, 104, 4681–4967, 1999.
- Masters, G., G. Laske, H. Bolton, and A. Dziewonski, The relative behavior of shear velocity, bulk sound speed, and compressional velocity in the mantle: Implications for chemical and thermal structure, in *Earth's Deep Interior: Mineral Physics and Tomography from the Atomic to the Global Scale*, *Geophys. Monogr. Ser.*, vol. 117, edited by S. Karato et al., pp. 63–87, AGU, Washington, D. C., 2000.
- Müller, R. D., W. R. Roest, J.-Y. Royer, L. M. Gahagan, and J. G. Sclater, Digital isochrons of the world's ocean floor, *J. Geophys. Res.*, 102, 3211–3214, 1997.
- Pyle, D. J., D. M. Christie, J. J. Mahoney, and R. A. Duncan, Geochemistry and geochronology of ancient southeast Indian and southwest Pacific sea floor, *J. Geophys. Res.*, 100, 22,261–22,282, 1995.
- Ritzwoller, M. H., and A. L. Levshin, Eurasian surface wave tomography: Group velocities, *J. Geophys. Res.*, 103, 4839–4878, 1998.
- Ritzwoller, M. H., N. Shapiro, A. Levshin, and G. M. Leahy, Crustal and upper mantle structure beneath Antarctica and surrounding oceans, *J. Geophys. Res.*, 106, 30,645–30,670, 2001.
- Ritzwoller, M. H., N. M. Shapiro, M. P. Barmin, and A. L. Levshin, Global surface wave diffraction tomography, *J. Geophys. Res.*, 107(B12), 2335, doi:10.1029/2002JB001777, 2002.
- Saxena, S. K., and G. Shen, Assessed data on heat capacity, thermal expansion, and compressibility from some oxides and silicates, *J. Geophys. Res.*, 97, 19,813–19,825, 1992.
- Sempere, J.-C., J. R. Cochran, and the SEIR scientific team, The Southeast Indian Ridge between 88°E and 118°E: Variations in crustal accretion at constant spreading rate, *J. Geophys. Res.*, 102, 15,463–15,487, 1997.
- Shapiro, N. M., and M. H. Ritzwoller, Monte-Carlo inversion of broadband surface wave dispersion for a global shear velocity model of the crust and upper mantle, *Geophys. J. Int.*, 151, 88–105, 2002.
- Shen, Y., and D. W. Forsyth, Geochemical constraints on initial and final depths of melting beneath mid-ocean ridges, *J. Geophys. Res.*, 100, 2211–2237, 1995.
- Smith, W. H. F., and D. T. Sandwell, Global seafloor topography from satellite altimetry and ship depth soundings, *Science*, 277, 1957–1962, 1997.
- Tolstoy, M., A. J. Harding, J. A. Orcutt, and J. Phipps Morgan, Crustal thickness at the Australian-Antarctic discordance and neighboring Southeast Indian Ridge, *Eos Trans. AGU, Fall Meet. Suppl.*, 76(46), Fall Meet. Suppl., F570, 1995.
- Trampert, J., and J. H. Woodhouse, Global phase velocity maps of Love and Rayleigh waves between 40 and 150 s period, *Geophys. J. Int.*, 122, 675–690, 1995.
- Veevers, J. J., Australian-Antarctic depression from the mid-ocean ridge to adjacent continents, *Nature*, 295, 315–317, 1982.
- Vogt, P. R., N. K. Cherkis, and G. A. Morgan, Evolution of the Australian-Antarctic Discordance from a detailed aeromagnetic study, in *Antarctic Earth Science: Proceedings of the 4th International Symposium on Antarctic Earth Sciences*, edited by R. L. Oliver, P. R. James, and J. Jago, pp. 608–613, Aust. Acad. Sci., Canberra, 1984.
- Weissel, J. K., and D. E. Hayes, Asymmetric spreading south of Australia, *Nature*, 213, 518–521, 1971.
- Weissel, J. K., and D. E. Hayes, The Australian-Antarctic Discordance: New results and implications, *J. Geophys. Res.*, 79, 2579–2588, 1974.
- Wessel, P., and W. H. F. Smith, Free software helps map and display data, *Eos Trans. American Geophysical Union*, 72(441), 445–446, 1991.
- Wessel, P., and W. H. F. Smith, New version of the Generic Mapping Tools released, *Eos Trans. AGU*, 76, 329, 1995.
- West, B. P., W. S. D. Wilcock, J.-C. Sempéré, and L. Géli, Three-dimensional structure of asthenospheric flow beneath the Southeast Indian Ridge, *J. Geophys. Res.*, 102, 7783–7802, 1997.
- Zhang, Y. S., and T. Tanimoto, High resolution global upper mantle structure and plate tectonics, *J. Geophys. Res.*, 98, 9783–9823, 1993.
- G. M. Leahy, Geology and Geophysics Department, Yale University, New Haven, CT 06520-8109, USA.
- M. H. Ritzwoller and N. M. Shapiro, Center for Imaging the Earth's Interior, Department of Physics, University of Colorado, Campus Box 390, Boulder, CO 80309, USA. (ritzwoller@ciei.colorado.edu)